ESTEC

European Space Research
and Technology Centre
Keplerlaan 1
2201 AZ Noordwijk
The Netherlands
www.esa.int

PERFORMANCE REPORT

The spectral calibration of JWST/NIRSpec: accuracy of the instrument model for the ISIM-CV3 test cycle

Prepared by G. Giardino and N. Luetzgendorf

Reference ESA-JWST-SCI-NRS-RP-2016-011
Issue/Revision 1.0
Date of Issue June 22, 2016
Status Released

European Space Agency
Agence spatiale européenne

APPROVAL

Title The spectral calibration of JWST/NIRSpec: accuracy of the instrument model for the ISIM-CV3 test cycle	
Issue Number 1	**Revision Number** 0
Author G. Giardino and N. Luetzgendorf	**Date** June 22, 2016
Approved by	**Date of Approval**
M.Sirianni	June 22, 2016

CHANGE LOG

Reason for change	Issue Nr.	Revision Number	Date

CHANGE RECORD

Issue Number 1	Revision Number 0		
Reason for change	**Date**	**Pages**	**Paragraph(s)**

DISTRIBUTION

Name/Organisational Unit
SCI-ODJ
ESTEC

Contents

1 INTRODUCTION

The NIRSpec parametric model is the backbone of the spatial and wavelength calibration of the spectra obtained with all the instrument spectroscopic modes: Fixed Slits, Multi-object spectroscopy (MOS), and Integral Field Unit (IFU). Although it was originally developed to make predictive "forward" simulations of NIRSpec data, once properly calibrated, the parametric model naturally also provides the geometrical transformations to i) enable the extraction of the spectra from NIRSpec images and to ii) aid the required computations for the on-board target acquisition procedure.

We have developed a procedure that uses the calibration data acquired for a limited subset of the NIRSpec modes - and in particular only 1.5% of NIRSpec's a quarter of a million slits - to fine-tune the parameters of the instrument model and we have demonstrated (Dorner et al. 2016) that the model can be calibrated with an accuracy well within requirements, using data acquired during NIRSpec Performance Verification and Calibration campaign, undertaken at the IABG testing facilities in Germany in 2013 (Birkmann et al. 2012).

Early in 2015, however, the Micro Shutter Assembly (MSA) and the Focal Plane Assembly (FPA) of NIRSpec have been replaced. The quadrants of the new MSA have a smaller number of stuck closed shutters (less than 10%) and the new FPA unit features two new H2RG detectors, which are not affected by the performance degradation problem of the older model Rauscher et al. (2014). Therefore, the instrument model needs to be updated to reflect the changes in the optical geometry of these elements as well as the overall instrument alignment. For this purpose, we acquired a new set of imaging and spectral reference data during the most recent cycle of cryogenic tests that NIRSpec underwent, together with the other three scientific instruments of JWST, in the Space Simulator Facility of NASA GSFC (Kimble et al. 2016), at the end of 2015 and beginning of 2016.

In this document, we summarize the procedure that we have undertaken to optimize the value of the model parameters using these recently-acquired data and present the results in terms of the accuracy of the model spatial and wavelength calibration.

2 THE OPTIMIZATION OF NIRSPEC PARAMETRIC MODEL

Fig. 1 provides a schematic depiction of NIRSpec optical design and identifies its main optical elements, which are encapsulated in the NIRSpec parametric model. These are: the FORE optics which re-image the telescope image plane (OTEIP = optical telescope element image plane) onto the slit plane, the Filter Wheel Assembly (FWA) located in the pupil of the FORE, the MSA in the slit-plane, the collimator optics (COL) that project the light from the slits onto the Grating Wheel Assembly (GWA), the disperser elements (gratings and prism) and the mirror housed in the GWA, the camera optics (CAM), and the FPA. The IFU entrance aperture is located in the MSA plane; the IFU optics are split into an IFU FORE part, which reimages and rescales the MSA plane onto the slicer, and an IFU POST part, which picks up the 30 image parts and creates a virtual image for each slice at the MSA plane (virtual slits).

There are two types of components in the NIRSpec parametric model: the parameterization of the coordinate transforms between the principal optical planes (here COL, IFU FORE, IFU POST, and CAM) and the geometrical description of the key plane elements (MSA, IFU slicer, GWA, and FPA). The coordinate transforms consist of a paraxial transform between the principal planes, plus two fifth-order, two-dimensional polynomial that model the distortions in x and y – see Giardino (2013) and Dorner et al. (2016) for a detailed description of the model elements and the list of free parameters (that are more than 300 in total). Although, the parametric model encapsulates all of the main optical elements identified in Fig. 1, the work presented here is limited to the optimization of the parameters describing the spectrographic part of NIRSpec, that is the instrument from the MSA to the FPA.

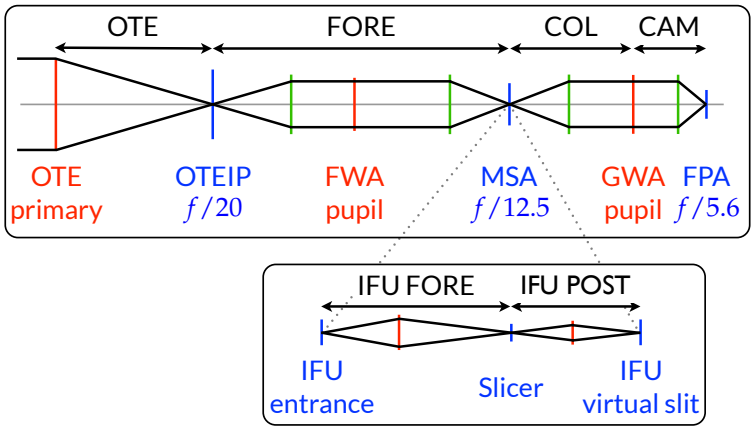

Figure 1: Paraxial layout of the JWST telescope and NIRSpec optical train with elements at principal planes, and the insert for the IFU case. Focal planes are blue, pupil planes red. All these elements are encapsulated in the NIRSpec parametric model.

2.1 The reference data set

The main principle underlying the model optimization consists in adjusting the many model parameters to minimize the distance between the model-computed and the measured location of a set of spectral lines and aperture images (the reference data), in the NIRSpec main optical planes.

Because NIPS uses the transforms of the parametric model, the optimization of the model has to follow an iterative approach. So, the images and spectra from the calibration exposures are extracted from the count-rate images with an increasing level of accuracy in terms of wavelength and spatial location at the FPA, as one proceed through the various steps of the overall procedure for the model calibration. This involves a first, so called "manual adjustment" step, in which large differences between predicated and observed images and spectra location in the detector-arrays are adjusted by manually entering appropriate coordinate off-sets (e.g of the quadrants location) and a second, "global model optimization" step in which the model free parameters are simultaneously modified by a least square fit software to yield the best agreement between the model-computed and the observed positions of the reference images and spectral lines – see Dorner et al. (2016) for a detailed description of this procedure.

For the optimization of the NIRSpec parametric model three types of data are necessary: imaging data, continuum spectra, and spectral lines. The first two sets provide spatial reference data, while the last one is used to derive spectral references. For the imaging mode, we acquired exposures of the MSA, illuminated by the CAA TEST lamp, in a checkerboard pattern. The imaging reference data comprise the positions of all fixed-slit and IFU virtual slit images, plus a subset of the MOS aperture (roughly 6000).

For spatial reference of the spectral modes, we used the CAA sources FLAT1, FLAT2, and FLAT3 that provide blackbody spectra for the three wavelength ranges $1.0 - 1.8$ μm, $1.7 - 3.0$ μm, and $2.9 - 5.0$ μm, matched to the NIRSpec bands. The spectral references are provided by the CAA sources REF, which is a rare earth absorption line source (Erbium) with absorption features in the $1.4 - 1.6$ μm wavelength range, and LINE1, LINE2 and LINE3, that employ Fabry-Perot type interferometric filters to provide five well defined transmission features over Band I, II, and III. All the CAA sources provide a spatially uniform illumination of the NIRSpec slit plane.

For each grating selection, 3 sets of 4 exposures with the MSA configured in four different patterns of multiple dashed-slits were acquired, one set illuminated by the continuum flat field lamp appropriate for that grating, the

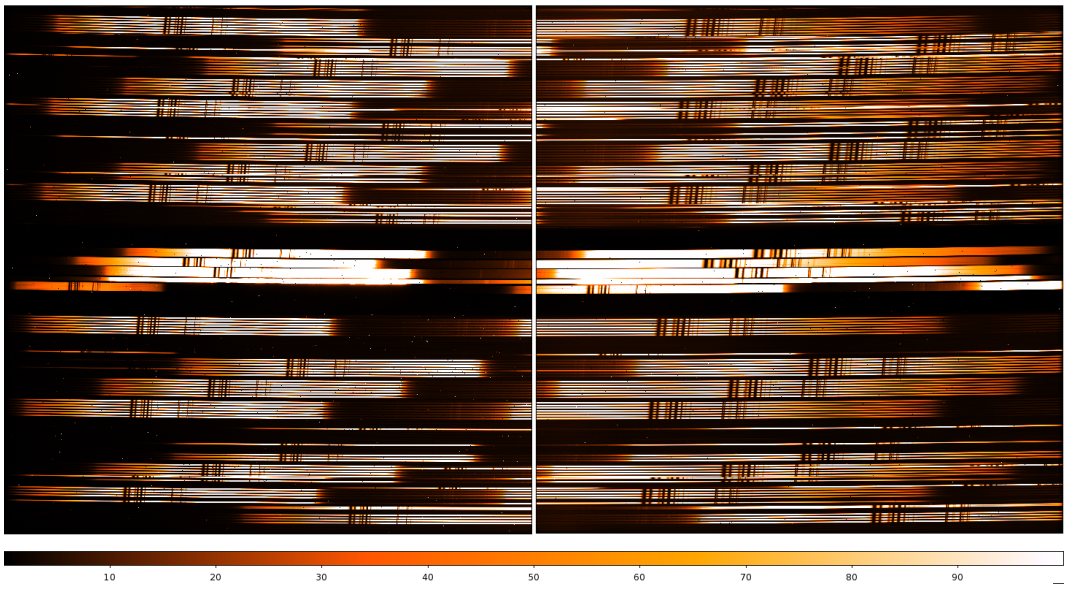

Figure 2: Count-rate images of the two NIRSpec detector arrays of an exposure of the REF lamp acquired with G395H (second and third order are visible) and the MSA configured in a dashed slit pattern. In this case the dashed slits were open in Q3 and Q4. The regular pattern of spectra is spoiled by the missing spectra due to shutters that fail to open, or by misaligned, overlapping spectra from shutters that cannot be closed (stuck open). The image was generated from NIRSpec raw data using our pre-processing pipeline.

second set illuminated with the appropriate LINE lamp, and the third one using the REF lamp, in the gratings' second and third order for band II and III gratings. A so-called dashed-slit consists of 14 shutters in a column, where an open shutter is followed by a closed one, yielding seven open shutters per slit. The four patterns were chosen to homogeneously sample the MOS FOV. We placed ten dashed slits distributed in each quadrant, using alternatively Q1 and Q2, or Q3 and Q4. Fig. 2 provides an image of REF spectra taken with one of the four MSA dashed-slit patterns and grating G395H.

For the prism we acquired multiple exposures of LINE1, LINE2 and LINE3 to cover the entire bandwidth, with the detector in stripe read-out mode to prevent saturation from the bright sources. In this case, only one MSA multiple dashed-slit configuration was adequate to distribute the spectra homogeneously across the entire focal plane.

Note that unlike for the calibration of the instrument model performed with data collected in 2013, this time we did not have access to an Argon spectral line source. The absorption and emission features of the NIRSpec internal sources were calibrated to the required tenth-of-a-nanometer level of accuracy from spectra acquired during the 2013 campaign, wavelength calibrated using this model-based approach (Dorner et al. 2016). The stability in time and with operating temperatures of the wavelength of the CAA sources spectral features was verified using the calibration data set from 2013 (Giardino 2014).

For each exposure, the count-rate images were derived from the raw exposure data using the pre-processing pipeline Birkmann (2011) with default settings. This involves the following steps: bias subtraction, reference pixel subtraction, linearity correction, dark subtraction,[1] and up-the ramp fitting, as described in more detail in Birkmann (2011) and Böker et al. (2012). Exposures of the LINE lamps where flat-fielded with the matching continuum exposures.

Using NIPS, spectral traces from the fixed-slits, MSA microshutters, or the IFU were extracted from the count-

[1] Dark subtraction is carried out at the data cube level, i.e., the corresponding frame from a low-noise dark-currents cube is subtracted from each frame of the exposure.

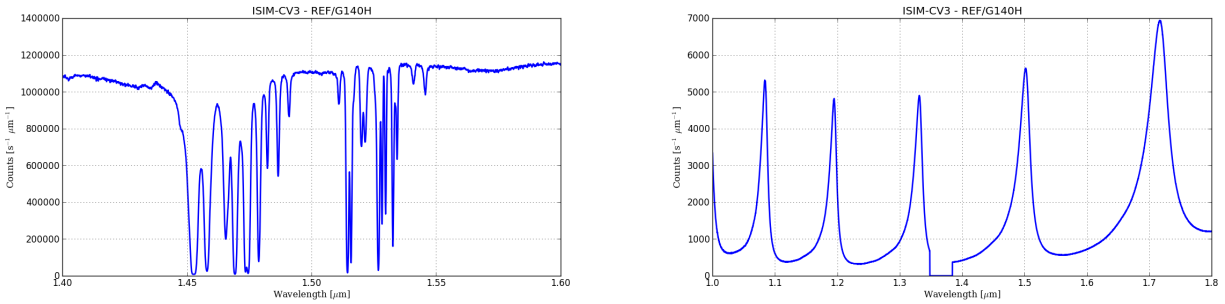

Figure 3: The spectra of two of the NIRSpec internal calibration sources REF (left) and LINES1 (right), taken with G140H. The Center of Gravity of the absorption and emission features of these sources were used as reference points for the optimization of the instrument's parametric model. No data are available for the spectrum of LINES1 around 1.35−1.38 μm, because in this range the light falls onto the gap between the two detectors (for this slit and grating combination).

rate images, rectified and collapsed to 1D-spectra (flux versus wavelength) computing the median along the spatial direction in each wavelength bin. The spectra were oversampled in spectral direction[2] to a final resolution of 2.5 times the Nyquist sampling of a grating's nominal resolution. Fig. 3 shows the spectra of REF and LINE1, as extracted from NIRSpec data. The centroid of the absorption and emission features of the CAA sources was computed from the 1D-spectra using the center of gravity (CoG) method (Cameron et al. 1982).

At the end of this processing, the MOS spectral reference data sets comprise the FPA positions of roughly 20,600 spectral lines for the gratings and 1800 line positions for the prism. IFU images and spectra of REF, LINE3 and FLAT3 lamps with G395H were also acquired, for a total of roughly 500 data points.

2.2 The global optimization

After having collected all the reference points, the model optimization by least-square fit can be carried out in four consecutive stages. The first step consists in the optimization of the MSA (microshutters location), and FPA geometry, the orientation angles of 4 out of 6 gratings (M-gratings plus G395H), and the distortions of the camera and collimator coordinate transforms in the forward direction. This involves the optimization of 120 parameters and is performed by a least-square fit that minimize the distance of the measured and model-computed locations of the reference points at the FPA (imaging and spectral reference points for the four gratings). After this, the relative positions and orientation of the fixed-slit are adjusted also by minimizing the residuals at the FPA, with 15 free parameters. The three orientation angles of the two remaining H gratings and the prism are fit next, for a total of 9 free-parameters.

At this point all the parameters necessary to compute the light paths in NIRSpec spectrograph in the forward direction using the model transform (for MOS and fixed-slit modes) have been optimized and one can look at the level of the overall residuals at the FPA, for the imaging mode, for the gratings and the prism. The plot of the distribution of the residuals between model-predicted and measure locations of the reference points at the FPA, for all the gratings, is shown in Fig. 4. The histograms of the distribution of the residuals in dispersion and spatial direction at the FPA (respectively i and j) are given in Fig. 5. The results, in terms of mean and median of the residuals at the FPA in spatial and spectral direction, for all the modes are summarized in Table 1. The residuals are overall small, with a typical (median) amplitude less than 1/10 of a pixel for all the modes.

Fig.6 to Fig.13 shows the residual distribution at the FPA for each individual disperser and the mirror.

The last step of the optimization process consists of three stages: first, the optimization of the distortions of the

[2]This is possible because NIRSpec spectra are slightly tilted on the FPA

Table 1: Residuals on the detectors of the optimized model forward projection MSA-to-FPA of the reference points for the MIRROR, all the gratings combined, and the prism. Here i is for dispersion direction and j for spatial direction.

GWA elements	Residual / pixels i mean + RMS	j mean + RMS	median absolute
Mirror	0.000 ± 0.019	-0.002 ± 0.025	0.020
Gratings	0.000 ± 0.092	0.002 ± 0.031	0.059
Prism	0.010 ± 0.111	0.00 ± 0.045	0.090

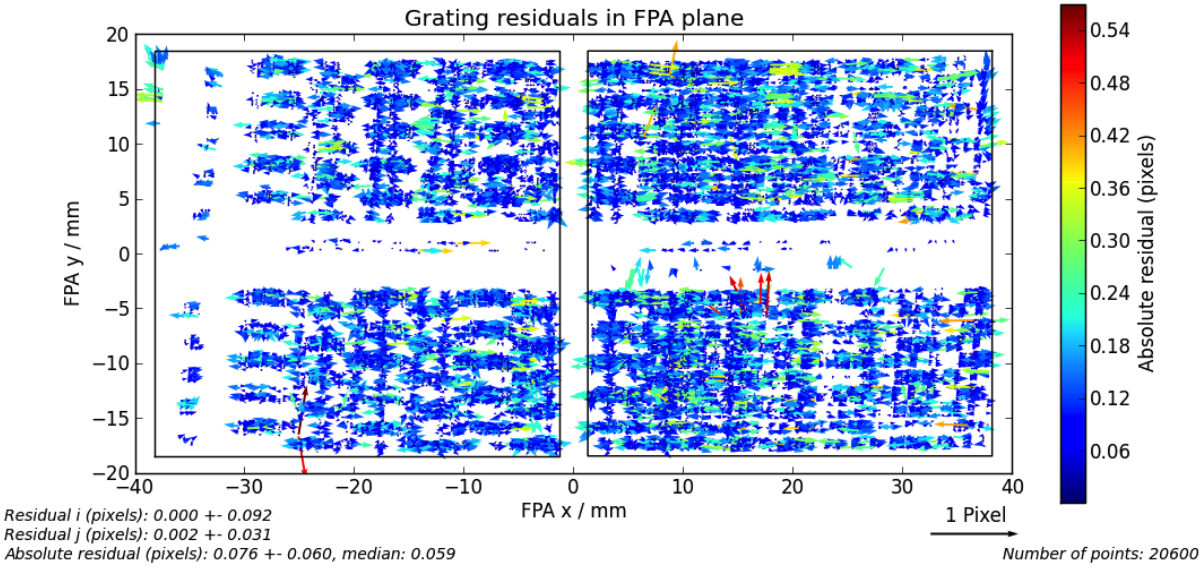

Figure 4: Residuals of forward coordinate transforms MSA-to-FPA, for all gratings on the detectors. The vectors give amplitude and direction of the difference between measured and model-computed location of the data points used to optimize 141 free parameters of the instrument model, specifically: MSA, FPA, tilt-angles for each grating and polynomial coefficients of the distortions of the COL and CAM transforms (see text).

CAM *backward* transform by minimizing the distance between predicted and measured locations of the reference points in the GWA exit plane; second, the optimization of the distortions of the COL *backward* transform by minimizing the distance between predicted and measured location of the reference points in the MSA plane and, finally, the optimization of the positions of the IFU virtual slits by minimizing the predicted and measured centroids of the 30 virtual slit images and spectral reference points from G395H – see also Dorner et al. (2016). Fig. 14 shows the distribution of the residuals at the FPA for the IFU reference points.

3 RESULTS AND DISCUSSION

With the model fully optimized in forward and backward direction, one can now evaluate the accuracy of the model wavelength calibration by looking at the residuals between the "true" wavelength of the reference lines and their values as measured in NIRSpec spectra, extracted using NIPS. The results are summarized in Table 2 for all the modes. The residuals (1-σ) RMS are at the level of 1/10 of a pixel or better, for all the grating modes, that correspond to a wavelength calibration accuracy of at least 1/20 of a resolution elements. This is two times

better than the formal standard deviation allocation of 0.2 pixel (or 1/10 of a resolution element) specified for this step in the overall wavelength calibration budget of NIRSpec. For the prism, the model accuracy is at the level of a 1/14 of a resolution element, also well within the requirements.

Table 2: Residuals between the 'true' wavelengths (CoGs) of the spectral features of the REF and LINES sources and those measured in the NIRSpec spectra extracted using the optimized parametric model (via NIPS). The values are average and RMS of the difference between the two quantities, over many lines, from MOS, fixed slit and IFU spectra

	Residual [pixel]			Residual [nm]		
Disperser	SLIT	MOS	IFU	SLIT	MOS	IFU
G140H	0.042 ± 0.047	-0.005 ± 0.083	-0.019 ± 0.046	0.010 ± 0.011	-0.001 ± 0.020	-0.004 ± 0.011
G235H	0.033 ± 0.051	-0.011 ± 0.097	-0.073 ± 0.049	0.013 ± 0.020	-0.004 ± 0.039	-0.029 ± 0.020
G395H	0.043 ± 0.080	0.007 ± 0.095	-0.010 ± 0.068	0.029 ± 0.054	0.005 ± 0.063	-0.007 ± 0.046
G140M	0.018 ± 0.052	0.004 ± 0.102	-0.041 ± 0.061	0.012 ± 0.033	0.003 ± 0.065	-0.026 ± 0.039
G235M	0.035 ± 0.046	-0.003 ± 0.075	-0.072 ± 0.042	0.038 ± 0.049	-0.003 ± 0.079	-0.076 ± 0.045
G395M	-0.009 ± 0.070	-0.014 ± 0.073	-0.058 ± 0.064	-0.017 ± 0.126	-0.026 ± 0.131	-0.104 ± 0.116
PRISM	-0.003 ± 0.061	-0.006 ± 0.135	-0.075 ± 0.134	-0.033 ± 0.884	-0.177 ± 2.142	-1.271 ± 2.155

The model accuracy obtained in this work is very similar to the results of the first iteration of the model calibration that was performed by Dorner et al. (2016), using calibration data acquired in 2013, when NIRSpec was not yet in its flight configuration. Those results were obtained having access to an Argon source which provided ideal spectral references. The results presented here provide the necessary update to the parameters of the instrument model now that NIRSpec is in its flight configuration and quantify the intrinsic wavelength calibration accuracy of this new version of the model. The fact that we reach here similar level of accuracies as in the previous work is a confirmation of the reliability and robustness of this model-based method of calibrating NIRSpec. Importantly, these results also establish that the CAA sources provide adequate spectral reference for the instrument wavelength calibration process.

The accuracy of the model for the spectrographic part of the instrument is a crucial part in the overall process of the NIRSpec wavelength calibration, but it is not the only part. There are two other important contributors to the overall wavelength calibration budget: the calibration of the spectrum shift caused by the finite repositioning accuracy of the grating wheel and the mixing of spatial and spectral information when our apertures are significantly larger than the size of the point-spread function (so-called slit effect). Concerning the grating wheel-induced shift, preliminary results (De Marchi et al. 2012) have shown that there is a tight linear relation between the telemetry readings of the GWA sensors and the tilt of a disperser element. These calibration relations are implemented during the spectral extraction to correct for the actual disperser orientation. Current analysis using ground test data shows that this correction leads to an additional contribution to the uncertainty of the wavelength calibration of approximately 1/16 of a pixel, which is a fraction of the model uncertainties.

Ultimately, for sky observations, the optical paths through the FORE elements of NIRSpec also have to be calibrated. This, however, has to be combined with the calibration of the telescope optics, thus it will be carried out once the instrument is in space, during the commissioning period. Using the data acquired from observations of an astrometric field in imaging mode, the parameters of the FORE transform for each filter element in combination with that for the OTE will be determined. This step will complete the spatial and spectral calibration of NIRSpec prior to the start of any scientific activity.

4 REFERENCES

Birkmann, S. 2011, Description of the NIRSpec pre-processing pipeline, NIRSpec Technical Note NTN-2011-004, ESA/ESTEC

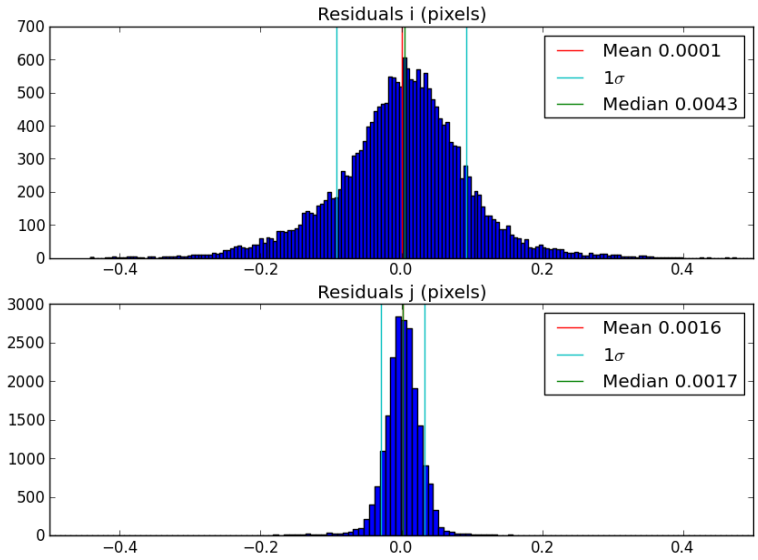

Figure 5: Distribution of the residuals of the forward coordinate transforms MSA-to-FPA after model optimization, for all the gratings, in i (dispersion) direction and j (spatial) direction (see text).

Birkmann, S. M., Ferruit, P., Böker, T., et al. 2012, in Society of Photo-Optical Instrumentation Engineers (SPIE) Conference Series, Vol. 8442, Society of Photo-Optical Instrumentation Engineers (SPIE) Conference Series, 3

Böker, T., Birkmann, S., de Marchi, G., et al. 2012, in Society of Photo-Optical Instrumentation Engineers (SPIE) Conference Series, Vol. 8442, Society of Photo-Optical Instrumentation Engineers (SPIE) Conference Series, 3

Cameron, D. G., Kauppinen, J. K., Moffatt, D. J., et al. 1982, Applied Spectroscopy, 36, 245

De Marchi, G., Birkmann, S. M., Böker, T., et al. 2012, in Society of Photo-Optical Instrumentation Engineers (SPIE) Conference Series, Vol. 8442, Space Telescopes and Instrumentation 2012: Optical, Infrared, and Millimeter Wave, 84423G

Dorner, B., Giardino, G., Ferruit, P., et al. 2016, A&A, Accepted

Giardino, G. 2013, An introduction to the NIRSpec parametric model, NIRSpec Technical Note NTN-2013-011, ESA/ESTEC

Giardino, G. 2014, The wavelength stability of the CAA sourcs across two test cycles of NIRSpec FM2, NIRSpec Performance Report NPR-2014-003, ESA

Kimble, R. A., Vila, M. B., Van Campen, J. M., et al. 2016, in Society of Photo-Optical Instrumentation Engineers (SPIE) Conference Series, Vol. This conference, Space Telescopes and Instrumentation 2016: Optical, Infrared, and Millimeter Wave

Rauscher, B. J., Boehm, N., Cagiano, S., et al. 2014, PASP, 126, 739

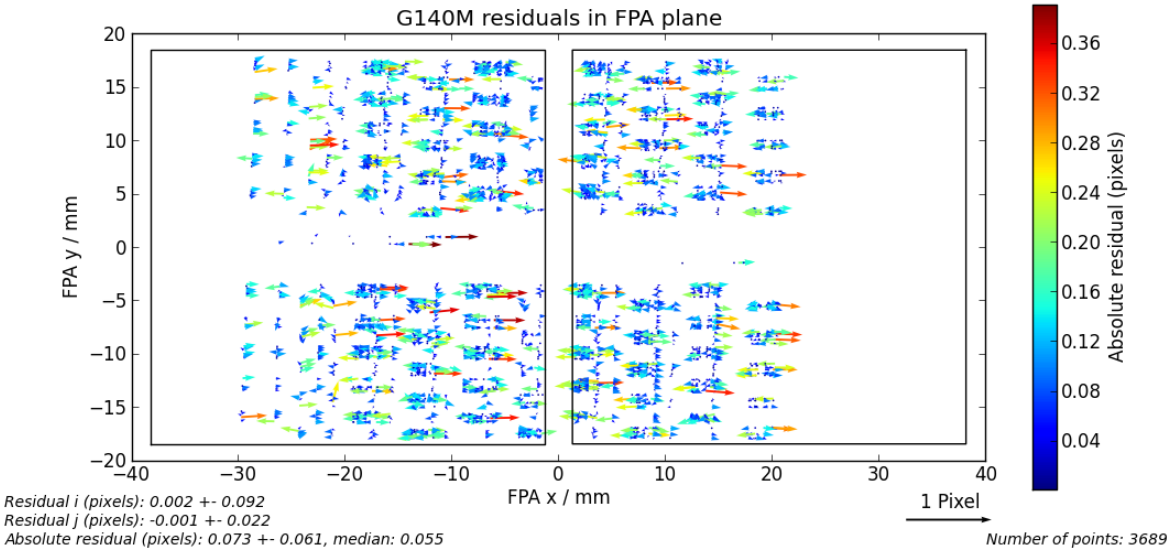

Figure 6: Residuals of forward coordinate transforms MSA-to-FPA, for G140M. The vectors give amplitude and direction of the difference between measured and model-computed location of the data points used to optimize the instrument model.

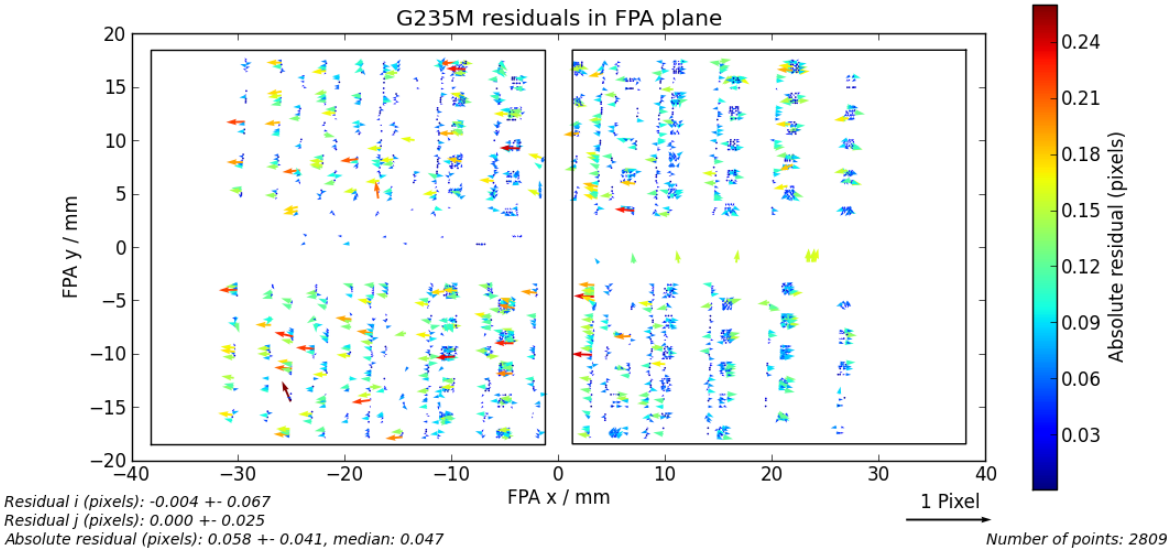

Figure 7: Same as Fig. 6 for G235M.

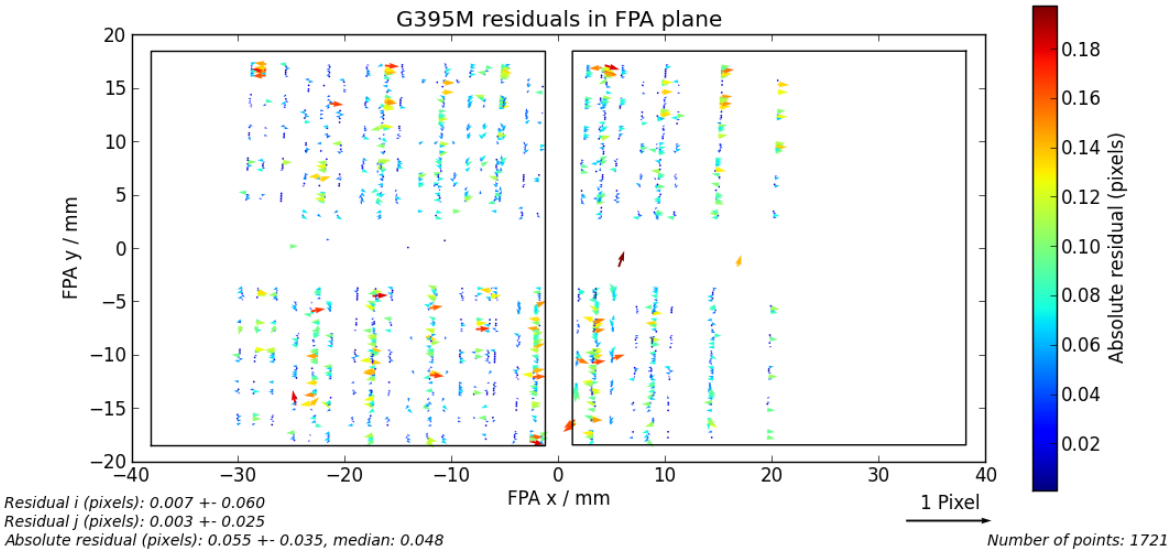

Figure 8: Same as Fig. 6 for G395M.

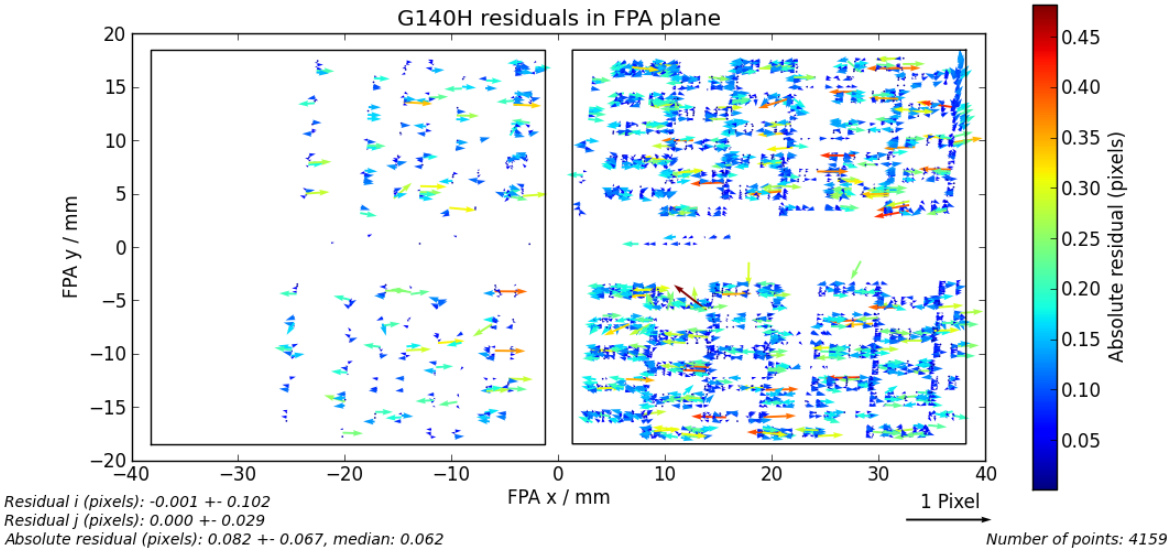

Figure 9: Same as Fig. 6 for G140H.

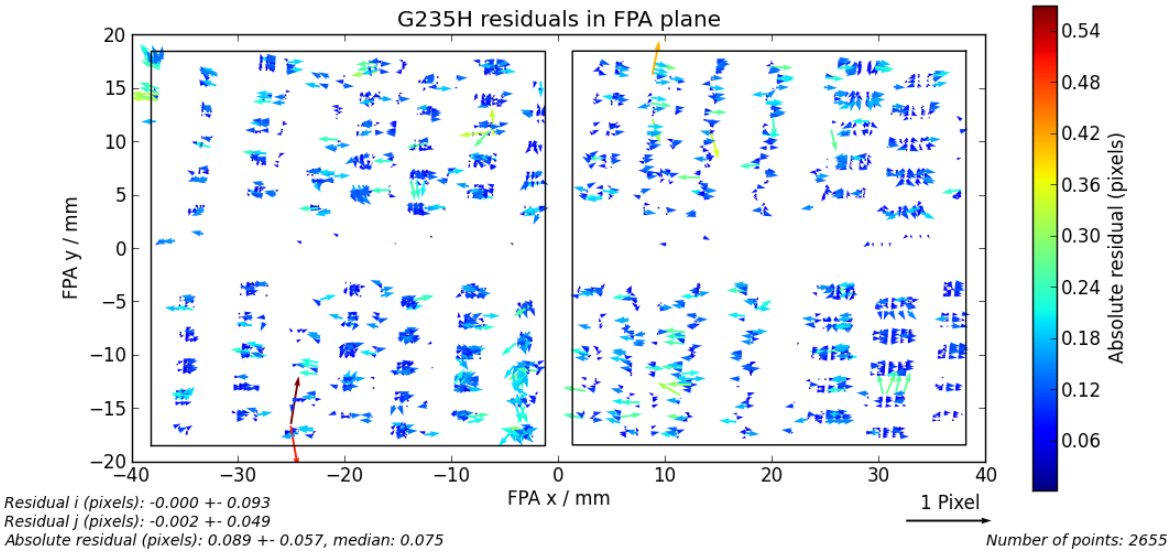

Figure 10: Same as Fig. 6 for G235H.

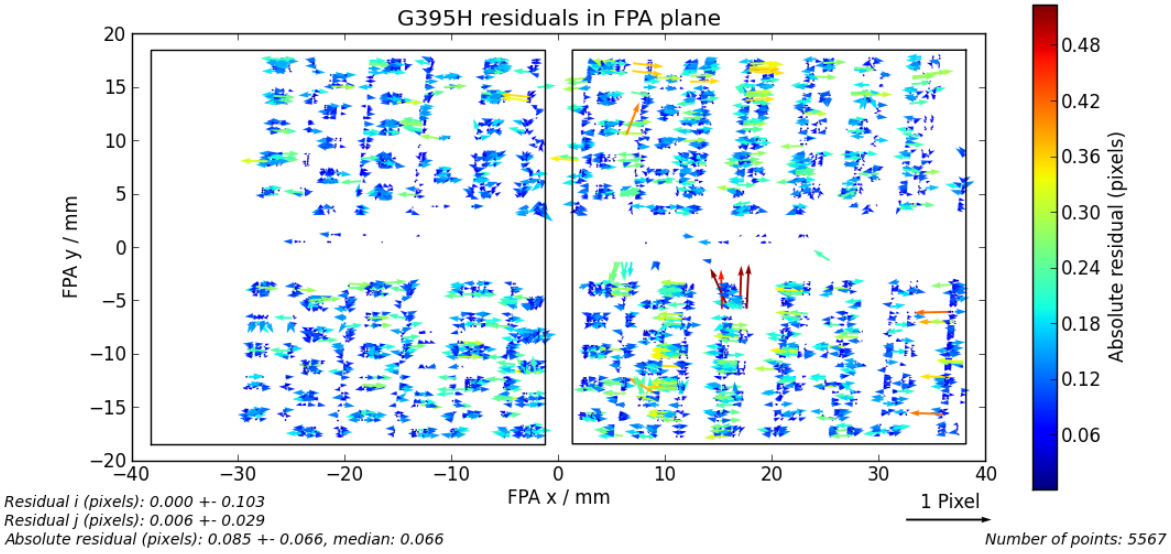

Figure 11: Same as Fig. 6 for G395H.

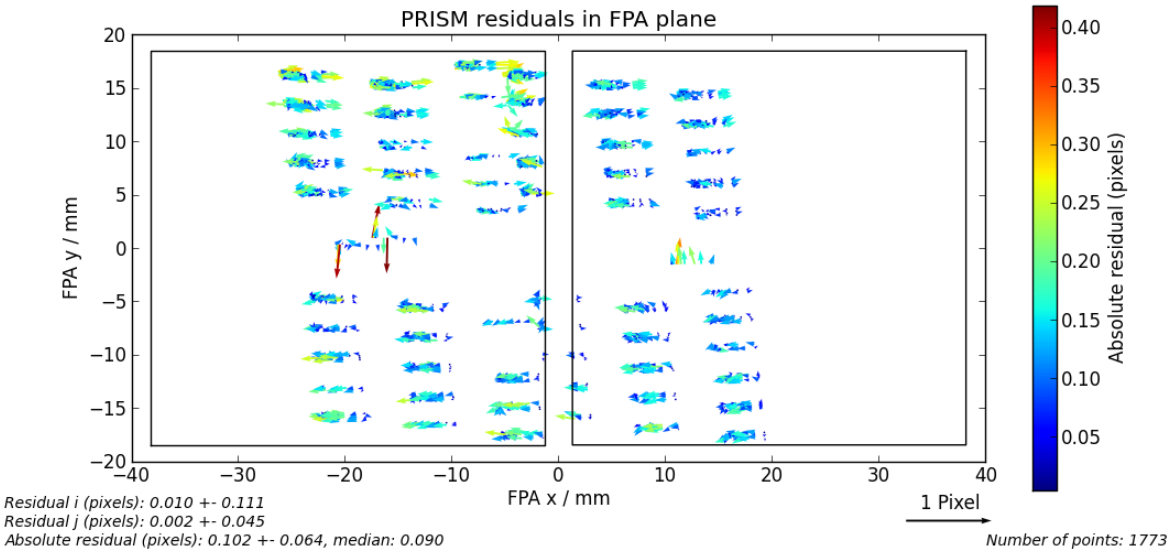

Figure 12: Same as Fig. 6 for the prism.

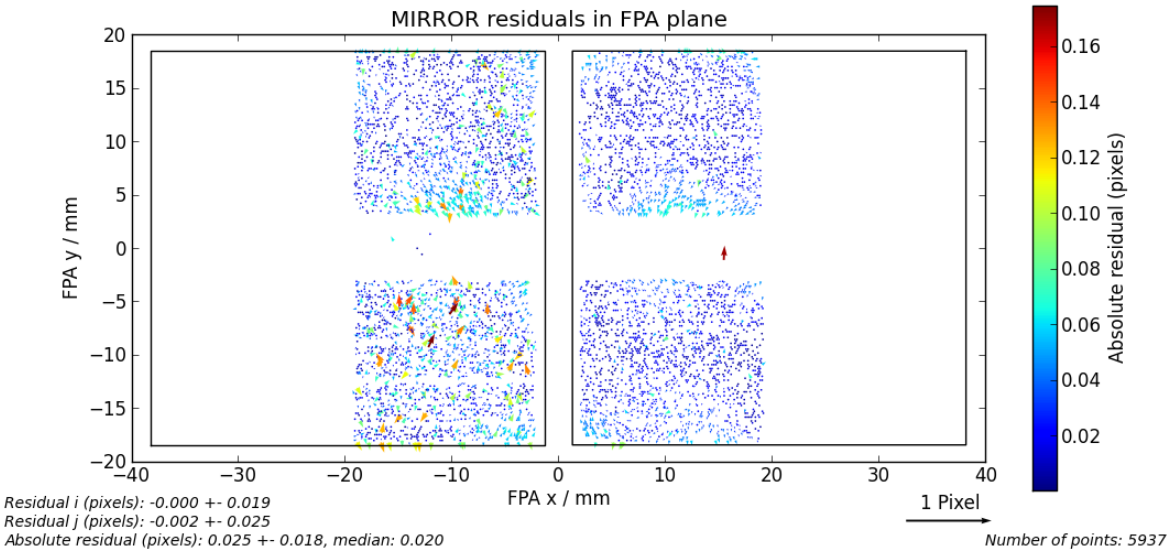

Figure 13: Same as Fig. 6 for the mirror.

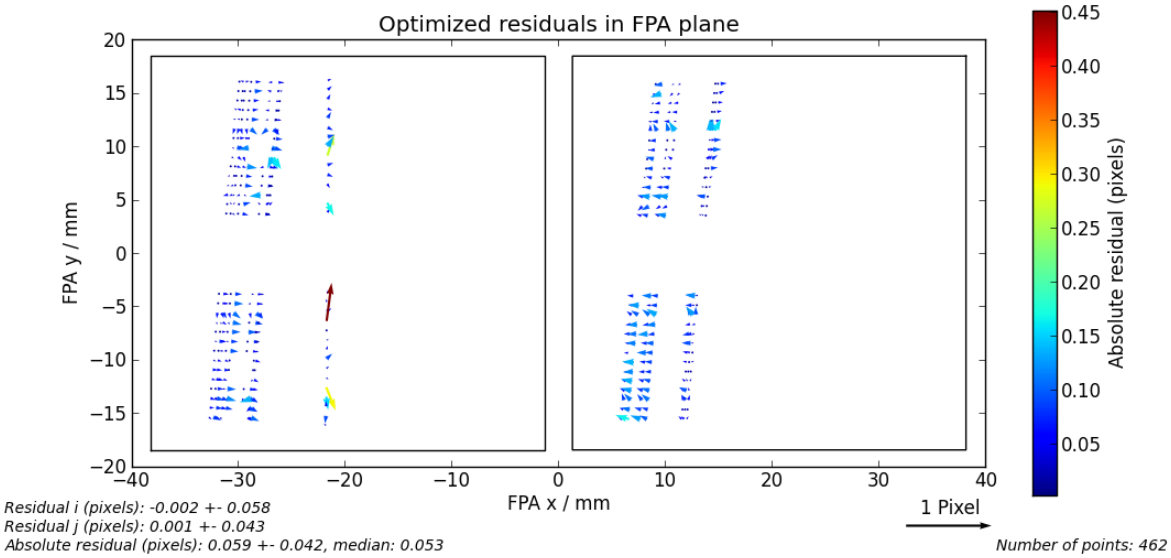

Figure 14: Same as Fig. 6 for the IFU (Imaging mode and G395H).